Science Advances
AAAS

advances.sciencemag.org/cgi/content/full/6/13/eaay4573/DC1

Supplementary Materials for

Emergence of a Neolithic in highland New Guinea by 5000 to 4000 years ago

Ben Shaw*, Judith H. Field, Glenn R. Summerhayes, Simon Coxe, Adelle C. F. Coster, Anne Ford, Jemina Haro, Henry Arifeae, Emily Hull, Geraldine Jacobsen, Richard Fullagar, Elspeth Hayes, Lisa Kealhofer

*Corresponding author. Email: ben.shaw@unsw.edu.au

Published 25 March 2020, *Sci. Adv.* **6**, eaay4573 (2020)
DOI: 10.1126/sciadv.aay4573

This PDF file includes:

Fig. S1. World map showing the centers where domestication of at least one plant species has occurred in the Early and Middle Holocene.
Fig. S2. Formally manufactured stone tools found on the surface or recovered during groundworks for gardening and house construction on the Waim spur by local residents before the archaeological investigations.
Fig. S3. Stratigraphic profiles, artefact density, and particle size analysis for the systematically excavated squares at Waim.
Fig. S4. Regional geology of the Simbai-Kaironk-Jimi Valleys showing the location of Waim and likely origins of excavated stone artefacts.
Fig. S5. Map of known stone mortar-pestle distribution and core distribution of stone carved bird iconography in Papua New Guinea and the adjacent islands relative to the location of Waim.
Fig. S6. Structural evidence and artefact distribution at the Waim site.
Fig. S7. Principal components analysis of Waim obsidian flaked piece and obsidian sources.
Fig. S8. Grassland mountains and forested Jimi River Valley landscape below Waim, looking south, with the Jimi-Wahgi divide in the background.
Fig. S9. The Waim site, looking east, situated on a natural hill top within Waim village.
Fig. S10. Excavation of the test pit showing the gabbro pestle fragment and other lithic artefacts exposed in the front (northern) half of the square.
Fig. S11. Partially exposed section that had been previously cut back by Waim residents around the northern edge of the hilltop.
Fig. S12. Square F after excavation showing a possible posthole feature in the lower right hand corner.
Fig. S13. The Waim site with the locations of the systematically excavated squares shown.
Fig. S14. Stone carving from square B, layer 2b.
Fig. S15. Artefact with incised cut/groove marks, from square B, layer 2c.
Fig. S16. Ground-stone fragments and corresponding microwear from various squares of the Waim excavations.
Fig. S17. Comparative reference starch used in this study and not shown in fig. S20.

Fig. S18. Dendrogram for the optimal classifier—a quadratic discriminant—showing the Mahalanobis distance between the means of the species.
Fig. S19. The confusion matrix for the reference species used in the study.
Fig. S20. Archaeological starch and their correlating species identification.
Fig. S21. Phytoliths identified on the Waim pestle and sediment.
Table S1. Radiocarbon determinations from Waim, mid-Holocene New Guinea highland sites, and the Holocene sequence from Kuk swamp (phases 1 to 3).
Table S2. Excavated lithic artefact assemblage from Waim, by square, layer, and artefact type.
Table S3. pXRF elemental concentrations (ppm; Ka1) for the Waim obsidian core and for the obsidian source samples.
Table S4. Numbers of grains identified of each of the comparative reference species.
Table S5. Error range of Bruker Tracer III-SD during analysis, using the U.S. Geological Survey BHVO-2 Geological Standard.
Table S6. Elemental loadings of three components (98% variation) for analyzed obsidian source samples and the Waim obsidian flake.
Text S1. Archaeological investigations at Waim
Text S2. Stratigraphic descriptions of sedimentary layers at Waim
Text S3. Technological and geological characteristics of the Waim lithics
Text S4. Microwear analysis of carved and modified lithic artefacts
Text S5. Geometric morphometric analysis of ancient starch from Waim
Text S6. Phytolith analysis of pestle and sediments from Waim
Text S7. pXRF reference data and principal components analysis of Waim obsidian
References (*44–69*)

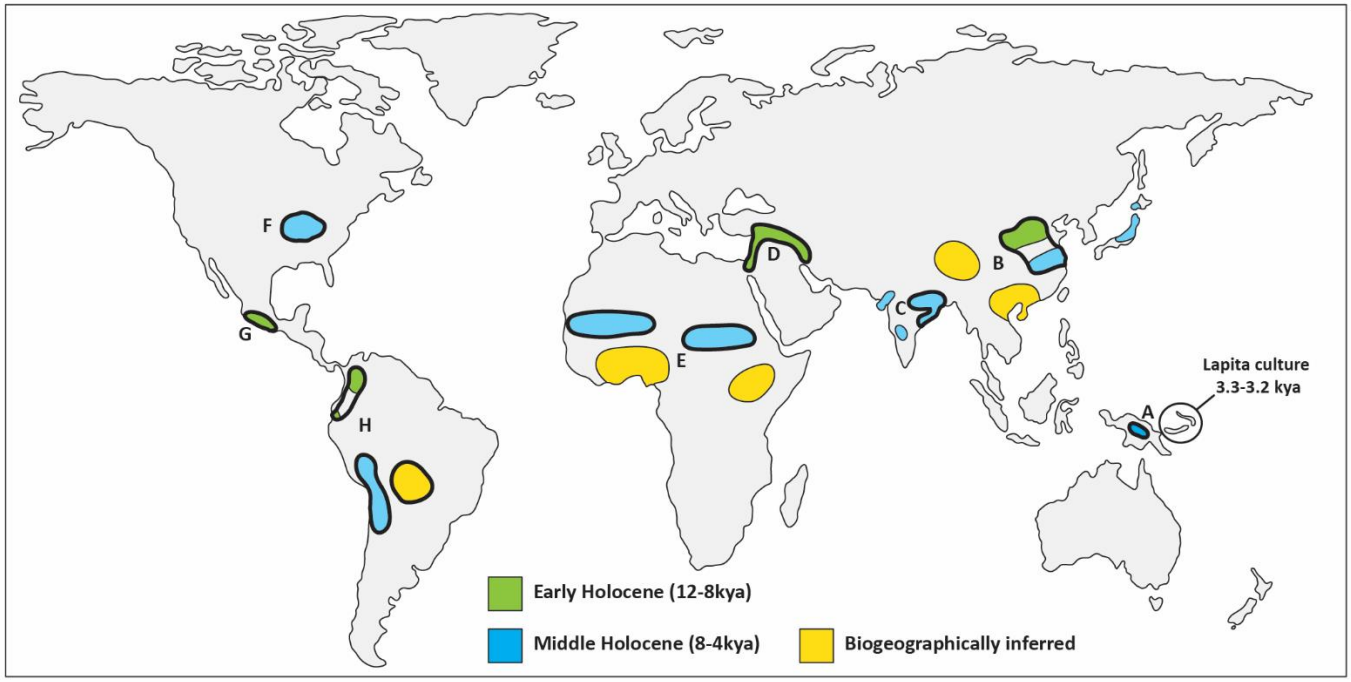

Fig. S1. World map showing the centers where domestication of at least one plant species has occurred in the Early and Middle Holocene. Bismarck Archipelago is circled where the earliest expression of Lapita culture is known. Areas with bolded lines indicate widely accepted independent centres for plant domestication/cultivation. Biogeographically inferred areas are where domesticated/cultivated plants are indigenous but found outside of their natural range. A = New Guinea, B = East Asia, C = South Asia, D = Southwest Asia (Near East), E = East Africa and South Arabia, F = North America, G = Meso-America, H=South America. Adapted from (*44*), Permission to adapt figure obtained from author. Figure Credit: Ben Shaw, UNSW.

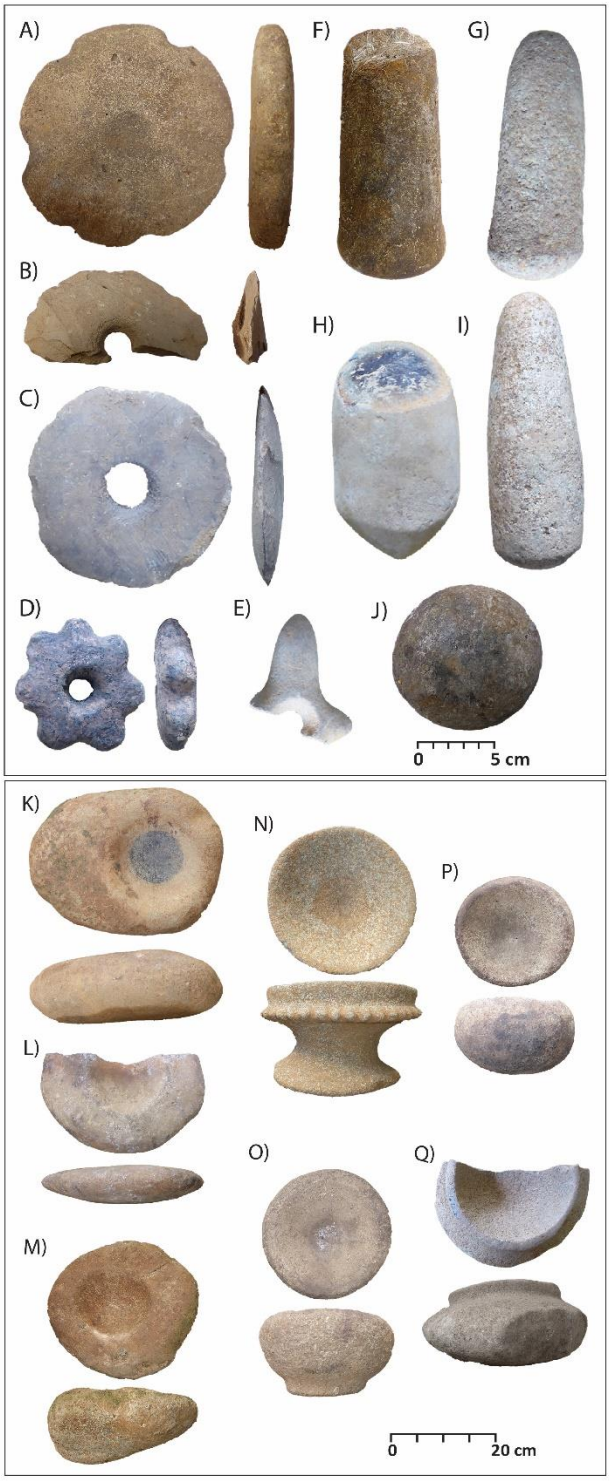

Fig. S2. Formally manufactured stone tools found on the surface or recovered during groundworks for gardening and house construction on the Waim spur by local residents before the archaeological investigations. A-**E**) Club heads, **F**-**I**) Pestles, **J**) Rounded grinding topstone. **K**-**M**) Mortars made from boulders. **N**) Pedestalled mortar with embossing. **O**) Pedestalled mortar. **P**) Mortar. **Q**) Mortar with lip. Photo and Figure Credits: Ben Shaw, UNSW.

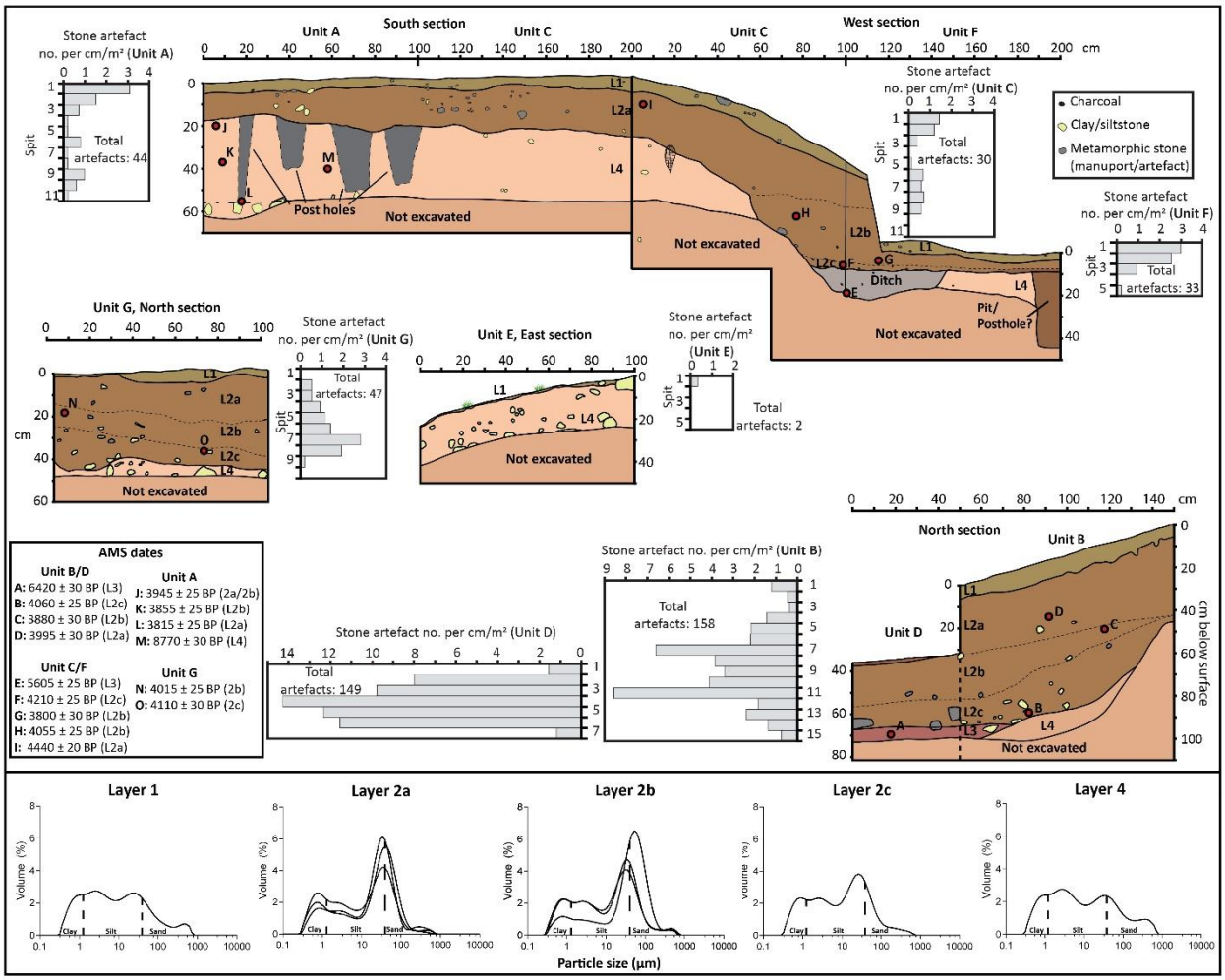

Fig. S3. Stratigraphic profiles, artefact density, and particle size analysis for the systematically excavated squares at Waim. Density was calculated by dividing the number of stone artefacts by the average spit depth (cm) and standardized to 1m^2 (0.01m^3). (Clay <2µm, silt: 2-63µm, sand: 63-2000µm). Particle size data for Layer 3 is not available. Layers 1 and 4 have a similar trimodal distribution of particle size because Layer 1 is re-deposited basal clay from modern stripping of the spur apex. Layer 2a-2c have a similar particle size distribution, with layers 2a-2b (multiple sediment samples) having a more pronounced peak of coarse silt and fine sand. Particle size within Layer 2a-c is consistent with the formation of a soil horizon and does not reflect a different stratigraphic context. Figure Credit: Ben Shaw, UNSW.

.

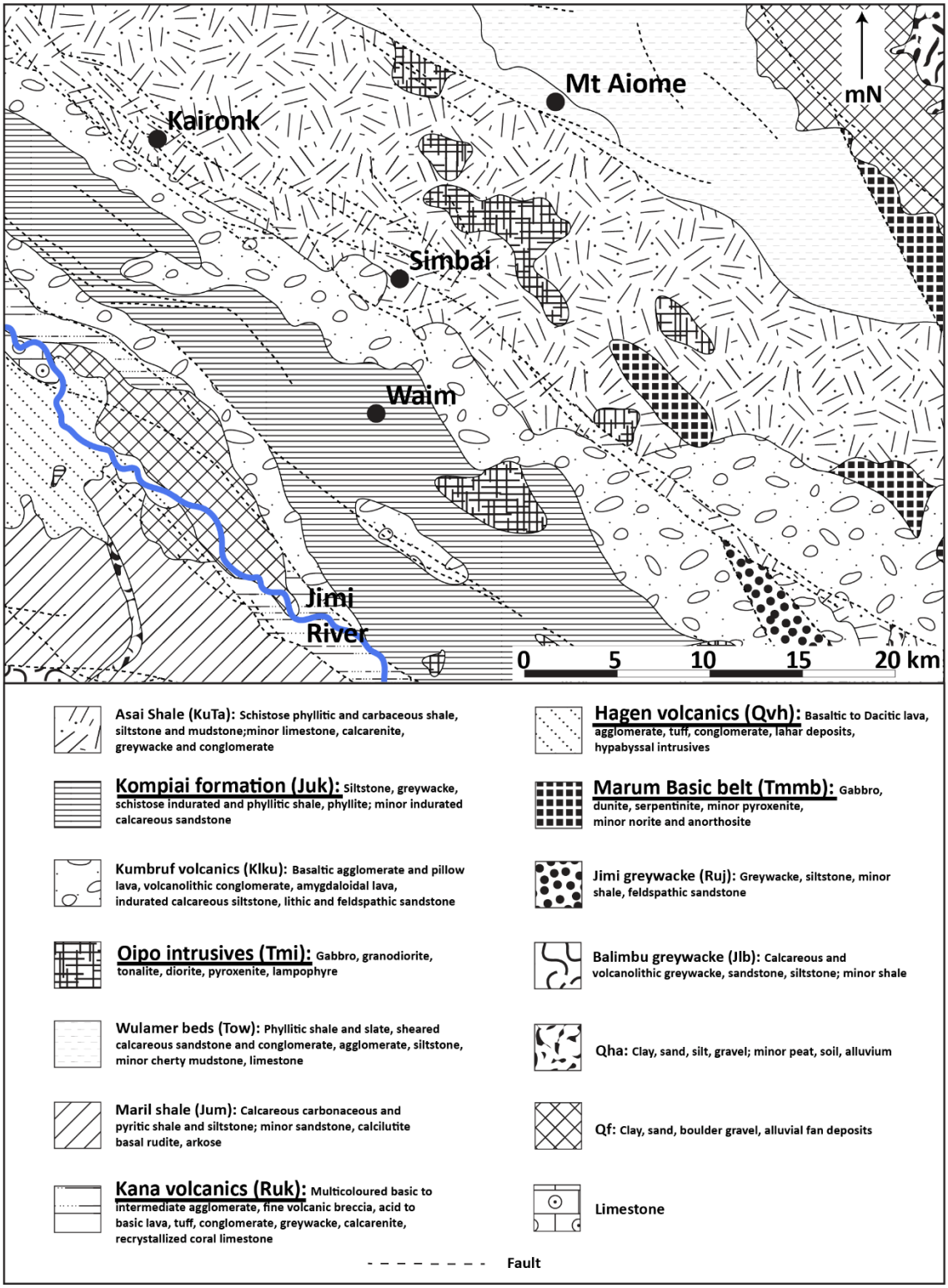

Fig. S4. Regional geology of the Simbai-Kaironk-Jimi Valleys showing the location of Waim and likely origins of excavated stone artefacts. Underlined units indicate the probable geological origins of excavated lithic artefacts. Adapted from an excerpt of 1:250 000 Papua New Guinea Geological Series map SB/55-5, Reference (*45*). Figure Credit: Ben Shaw, UNSW.

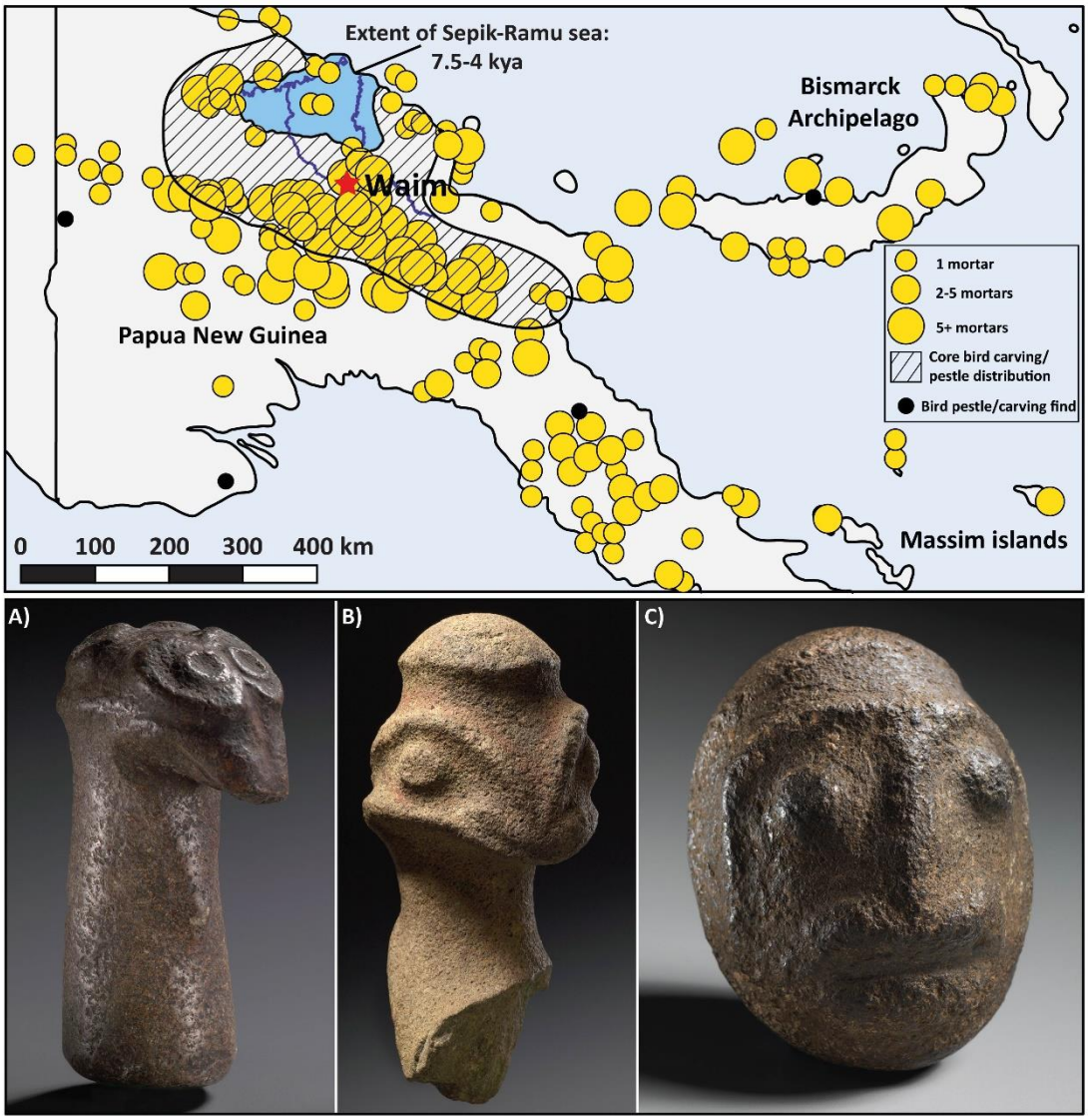

Fig. S5. Map of known stone mortar-pestle distribution and core distribution of stone carved bird iconography in Papua New Guinea and the adjacent islands relative to the location of Waim. **A**) Cassowary pestle pommel, Enga Province, Laiagam area, Lagaip River region. Stone (basalt). 12.7x5.1x7.6cm. JFA152.1. **B**) Cassowary pestle pommel, Enga Province, Maramuni area, near Kangirka village. Stone (possibly weathered andesite), red pigment. 27.9x14x15.2cm. JFA148. **C**) Anthropogenic head, Madang Province, Simbai Valley. Stone (basalt). 9.5x6.7x7.9cm. JFA511. Map redrawn from (*36*, *46*). Images of comparative carvings from (*47*). Photo Credits: ©2006 John Bigelow Taylor www.johnbigelowtaylor.com. Fine Arts Museum of San Francisco. Figure Credit: Ben Shaw, UNSW.

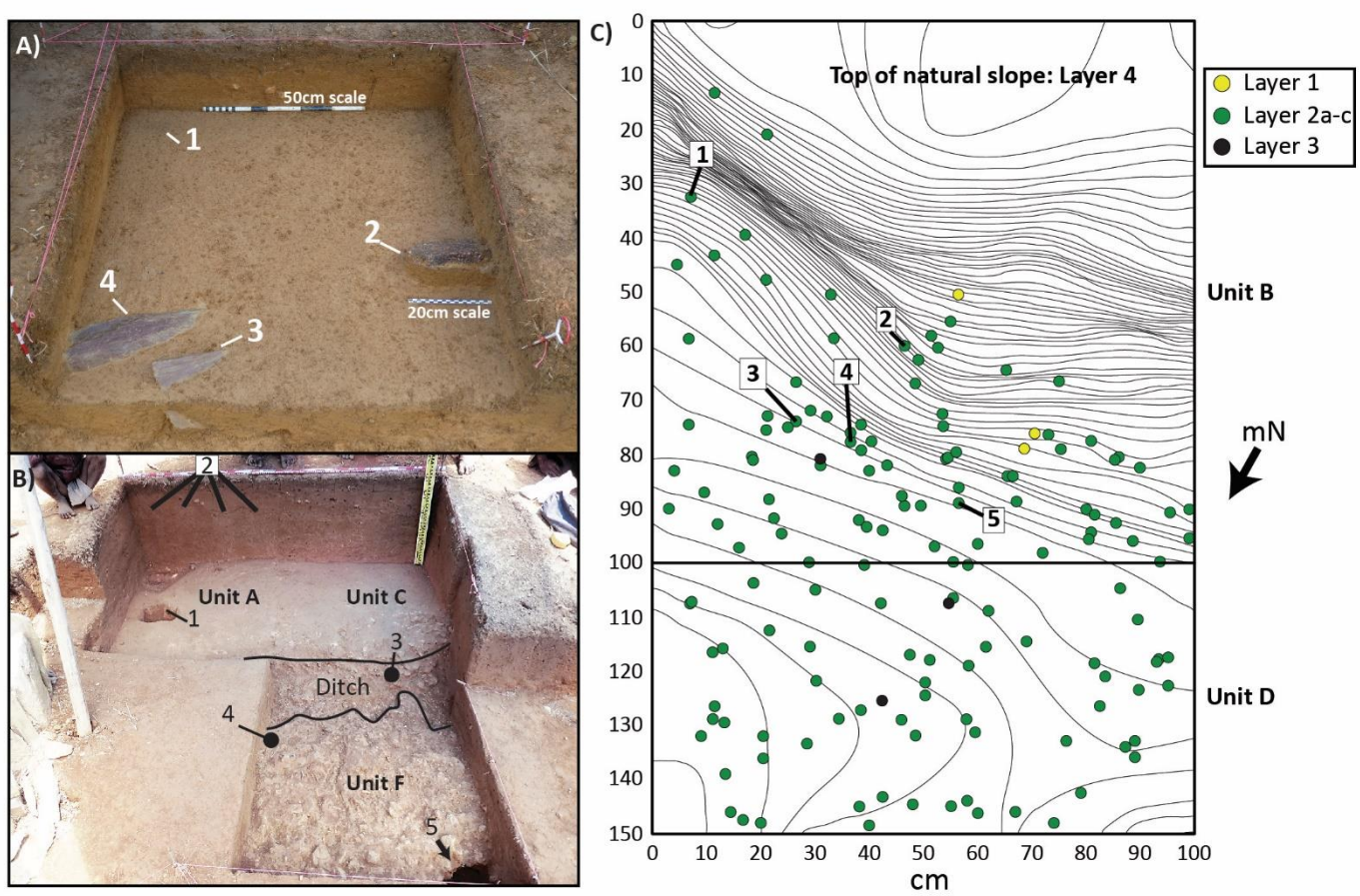

Fig. S6. Structural evidence and artefact distribution at the Waim site. A) Excavation of Layer 2a-2b in Square A on the slope showing the distribution of stone artefacts and features mentioned in text. 1: Darkened posthole fill, 2: Unmodified weathered and flat diorite rock cut into Layer 4. 3: Ground siliceous argillite planilateral axe-adze preform, 4: Siliceous argillite slab in initial stages of preform preparation. **B**) Completed excavation of Squares A, C and F showing features of mid-Holocene settlement. 1: Posthole A base, half-sectioned. 2: Postholes in section (Ø=10cm, 14cm, 17cm, 19cm, from Layer 2a cutting 40cm into Layer 4 basal clay). 3: Diorite pestle, Layer 2c. 4: Diorite-gabbro pestle, Layer 2b. 5: Possible large posthole, partially exposed. **C)** Distribution of stone artefacts recorded *in situ* by layer in Squares B and D. 1cm contours. 1: Carved stone fragment. 2: Volcanic rock with cutmarks and ochre residues. 3: Ground tool fragment. 4: Ground tool fragment. 5: Siliceous argillite with cut marks. Photo and Figure Credit: Ben Shaw, UNSW.

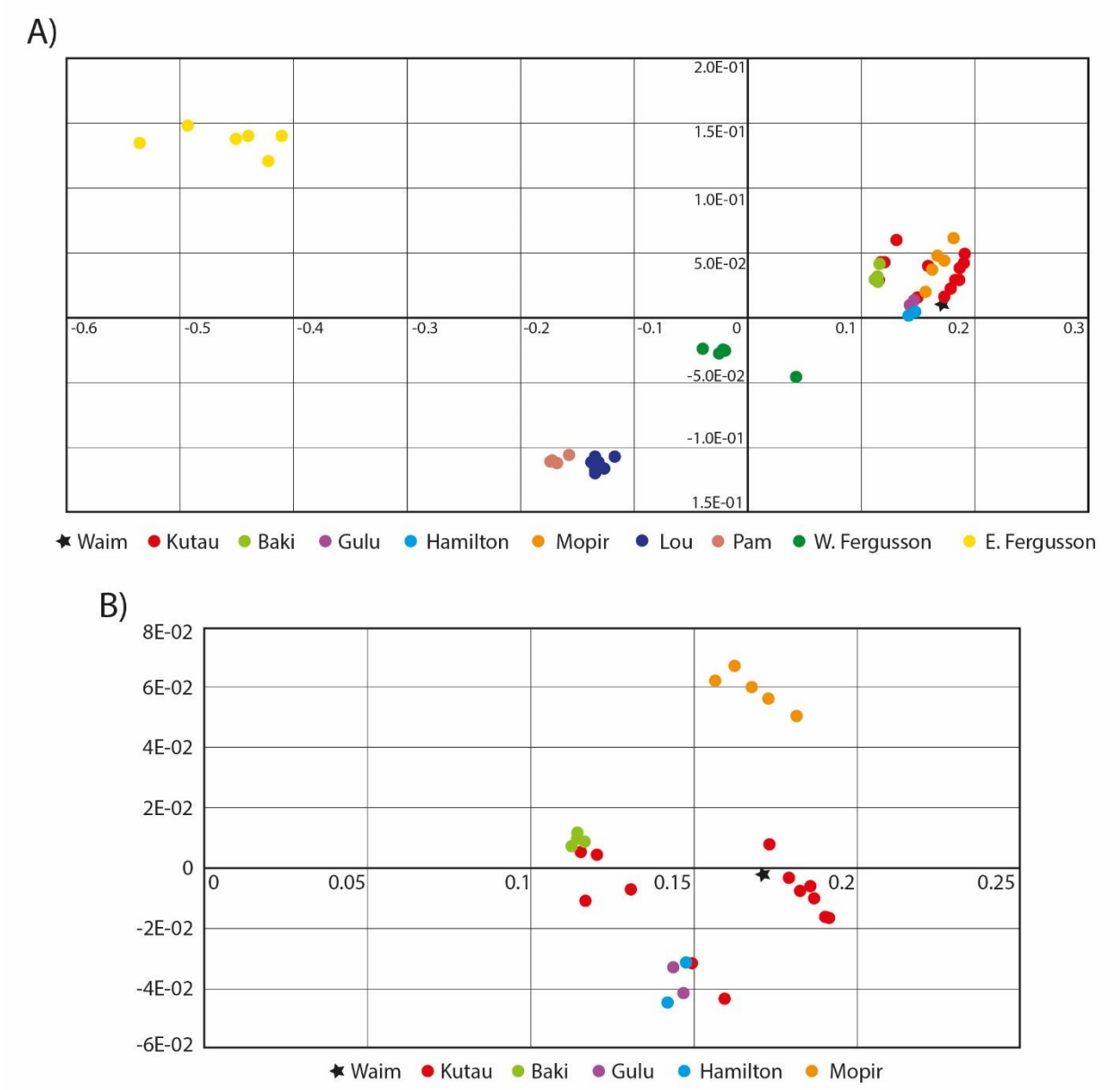

Fig. S7. Principal components analysis of Waim obsidian flaked piece and obsidian sources. A) first and second components including all New Britain, Manus and Fergusson obsidian source samples. **B**) First and third components including New Britain obsidian source samples only. The Waim obsidian piece (black star) clusters with Kutau source samples from New Britain (red dots). Figure Credit: Glenn Summerhayes.

Table S1. Radiocarbon determinations from Waim, mid-Holocene New Guinea highland sites, and the Holocene sequence from Kuk swamp (phases 1 to 3). Highlighted yellow dates are the earliest expression of Phase 3 rectilinear ditch systems, indicative of intensified wetland agricultural practices. Calibrated date ranges are displayed in Figure 2 of main text. CRA = Conventional Radiocarbon Age. Waim dates Calibrated using the IntCal13 curve and OxCal4.3. Table Credit: Ben Shaw.

Lab code	Area	Site	Site code	Context	δ13C	CRA	error	Material	Reference
Beta-450802	Jiwaka Province	Waim	WAA	Square A, Spit 9a, Layer 4	-26.6	8770	30	Charcoal	This study
Beta-450806				Square D, Spit 7, Layer 3	-24.8	6420	30	Charcoal	
OZU323				Square C, Ditch base	-23.9	5605	25	Charcoal	
OZW325				Square C, Spit 3b, Layer 2a	-26.4	4440	20	Charcoal	
OZU290				Square C, Spit 9a, Layer 2c	-28.6	4210	25	Charcoal	
Beta-450804				Square G, Spit 7, Layer 2c	-31.6	4110	30	Charcoal	
OZV222				Square B, Spit 14b, Layer 2c	-24.8	4060	25	Charcoal	
OZV226				Square C, Spit 7a, Layer 2b	-25.5	4055	25	Charcoal	
OZV227				Square G, Spit 4b, Layer 2b	-25.3	4015	25	Charcoal	
OZV221				Square B, Spit 6, Layer 2a	-25	3995	30	Charcoal	
OZV223				Square A, Spit 5, Layer 2a/b	-28	3945	25	Charcoal	
Beta-450805				Square B, Spit 9a, Layer 2b	-25.4	3880	30	Charcoal	
OZV224				Square A, Spit 9a, Layer 2b	-23.8	3855	25	Charcoal	
OZV225				Square A, Spit 11, posthole fill, Layer 2a	-26.1	3815	25	Charcoal	
Beta-450803				Square F, Spit 2, Layer 2b	-25.4	3800	30	Charcoal	
WK27070	Ivane	Vilakuav	AAXF	Layer 2		6240	30	Charcoal	(*48*)
WK27068						6070	32	Charcoal	
WK23357	Ivane	Joes Garden	AAXC	Layer 2		3938	34	Charcoal	(*48*)
WK23348						3855	30	Charcoal	
UW-108	Eastern Highlands	-	NGH	hearth		3780	120	Charcoal	(*26*)
RL-407	Eastern Highlands	-	NFB	6S6W, hearth		3960	170	Charcoal	(*26*)
Gak-623	Eastern Highlands	Aibura	NAE	Sq. IX, Level 2, Lower HIII		3800	110	Charcoal	(*19*)
ANU-1325	Wurup valley	Kamapuk		Level 15		4340	100	Charcoal	(*18*)
ANU-1373	Wurup valley	Manim	MJJ	Level 21		5860	130	Charcoal	(*18*)
ANU-1376				Level 34		5570	410	Charcoal	
I-6860	Kaironk	Wanelek	JAO	Area A, Unit 10A, layer 10		5455	105	Charcoal	(*49*)
Wk-22357				W/105Z/IV		4498	30	Charcoal	(*27*)
Wk-20409				Area B, Unit 17-18b, layer 11 (posthole)		4239	38	Charcoal	(*32*)
GX-3333b				Area A, Unit 11b, Layer 9		3840	175	Charcoal	(*49*)
Wk-22060				Area D, Unit 105Z, layer 5		3697	30	Charcoal	(*32*)
ANU-44	Hagen	Manton	MKK	Zone 2		4600	140	Wood digging stick	(*50*)
Y-1370	Western Highlands	Kiowa	MAH	1.5m, Level 6		6100	160	Ash	(*51*)
Y-1371				0.9m, Level 3		4840	140	Ash	
ANU-41a	Eastern Highlands	Kafiavana Cave	NBZ	260-310cm, over 6m2. Horizon VII-VIII		≥6750	100	Bone apatite	(*19*)
ANU-41b						10730	370	Bone collagen	
NZ1026				200-270cm, over 8m2. Lower Horizon VI to Horizon VII		9290	140	Bone collagen	
NZ1025						6180	125	Bone apatite	
ANU-42				Horizon II (base)		4690	170	Wood charcoal	
GX-3111a	Western Highlands	Yuku	MAH	Sq. 1A, Layer 3a		6710	265	Bone apatite	(*51*)
GX-3111b						4570	220	Bone collagen	
ANU-3688a	Chimbu Province	Nombe	NCA	Sq. X3, Stratum B		6740	120	Bone collagen	(*24*)
ANU-3688b						5880	210	Bone apatite	
ANU-3076				Sq. A1, Stratum B		5870	110	Bone apatite	
ANU-3075a				Sq. A1, Stratum B		6410	60	Bone collagen	
ANU-3075b						5900	110	Bone apatite	
ANU-3074a				Sq. A1, Stratum B		5030	110	Bone apatite	
ANU-3074b						5030	110	Bone collagen	
ANU-3684				Sq. J71, Stratum B		5340	120	Bone collagen	
ANU-3689				Sq. PQR71, Stratum B		5090	220	Bone collagen	
Wk-22081				Sq. X2.11, Stratum B		5442	30	Aggregate charcoal	(*52*)
Wk-22088				Sq. X2.11, Stratum D		4416	37	Aggregate charcoal	
Wk-22096				Sq. B3, Stratum B		6401	30	Aggregate charcoal	
Wk-22097				Sq. B3, Stratum A		4823	30	Aggregate charcoal	
Wk-31640				Sq. B3, Stratum B		6212	27	Single charcoal	
Wk-31642				Sq. B3, Stratum A		4848	25	Single charcoal	
ANU-11070	Western Highlands	Kuk Swamp		Phase 1 palaeochannel		8840	240	wood charcoal	(*53*)
ANU-11071						9050	90	wood charcoal	
ANU-11072						9040	80	wood charcoal	
ANU-11182						8800	100	wood charcoal	
OZD928						9030	60	bark	
OZD929						8840	60	bulk sediment	
OZD922				Phase 1 palaeosurface feature		8430	90	bulk sediment	
ANU-11441						9390	40	pollen/charcoal	
ANU-1057				Phase 2 palaeosurface features		5970	80	wood	
ANU-1196a						5950	80	leaves and wood	
ANU-1196b						5400	230	leaves and wood	
ANU-1311						5790	100	charcoal	
ANU-11183				Earliest phase 3 curivlinear		4130	80	charcoal	
ANU-11432						4380	40	pollen/charcoal	
OZF239				Early phase 3 ditch		4000	30	pollen/charcoal	
OZF240						3780	50	pollen/charcoal	
ANU-1315				Phase 3 palaeochannel		3520	90	peaty clay, bulk	
ANU-1464a						3900	140	mud fines	
ANU-1464b						3600	80	peat fines	
ANU-1815						3470	170	wood	
ANU-8055				Late phase 3 ditch		2650	80	peaty clay	
ANU-8056						2480	80	organic clay	
ANU-11185						2890	80	charcoal	

Table S2. Excavated lithic artefact assemblage from Waim, by square, layer, and artefact type.
Table Credit: Anne Ford.

Unit	Layer	Artefact Type								Total Number	Weight (g)
		Tool	Tool/ preform	Used flakes/ fragments	Core tool	Core	Flake	Angular Fragment	Manuport		
A	1	1					4	8		13	22.77
	2a	1					3	11	1	16	1786.36
	2a/2b	1						3		4	16.86
	2b	1					1	5		7	20.49
	2c			1				3		4	2.36
Total		**4**	**0**	**1**	**0**	**0**	**8**	**30**	**1**	**44**	**1848.84**
B	1			1			2	4		7	10.24
	2a	5	1	6	1		27	24		64	316.8
	2b	3	1	4			25	19		52	1908.12
	2c	8		1			11	11		31	714.71
	3			1			2	1		4	7.71
Total		**16**	**2**	**13**	**1**	**0**	**67**	**59**	**0**	**158**	**2957.58**
C	1						4	4		8	17.06
	2a					1	6	3		10	22.64
	2a/2b						2	1		3	1.13
	2b			1			2	3		6	27.26
	2b/2c						2	1		3	1.86
Total		**0**	**0**	**1**	**0**	**1**	**16**	**12**	**0**	**30**	**69.95**
D	2b	9	2	4		1	40	24	2	82	1327.2
	2c	3	4	2			31	21	1	62	2779.93
	3					1	3	1		5	317.71
Total		**12**	**6**	**6**	**0**	**2**	**74**	**46**	**3**	**149**	**4424.84**
E	1							2		2	1.53
Total		**0**	**0**	**0**	**0**	**0**	**0**	**2**	**0**	**2**	**1.53**
F	1	1					9	4		14	10.9
	2b	2		1			5	5		13	198.86
	2c						3	3		6	8.58
Total		**3**	**0**	**1**	**0**	**0**	**17**	**12**	**0**	**33**	**218.34**
G	2a			2			3	2		7	8.72
	2b	2		2		1	7	4		16	132.94
	2c	2		1		1	15	5		24	75.56
Total		**4**	**0**	**5**	**0**	**2**	**25**	**11**	**0**	**47**	**217.22**
Unit C Spade Pit	1						1			1	0.47
	2a						1	3		4	8.59
	2c	3		2			1	2		8	606.8
Total		**3**	**0**	**2**	**0**	**0**	**3**	**5**	**0**	**13**	**615.86**
Exposed section	1	1					1			2	22.67
	2a					1	3	2		6	24.14
	2b							**1**		1	12.05
	2c							1		1	7.34
Total		**1**	**0**	**0**	**0**	**1**	**4**	**4**	**0**	**10**	**66.2**
Grand Total		**43**	**8**	**29**	**1**	**6**	**214**	**181**	**4**	**486**	**10420.36**
%		**8.8**	**1.6**	**6.0**	**0.2**	**1.2**	**44.0**	**37.2**	**0.8**	**100**	

Table S3. pXRF elemental concentrations (ppm; Ka1) for the Waim obsidian core and for the obsidian source samples. Table Credit: Anne Ford and Glenn Summerhayes.

Sample code	Location	Mn	Fe	Ga	Rb	Sr	Y	Zr	Nb
Waim	Waim	390	11081	17	54	185	21	139	4
ANU1874	Talasea	419	7366	13	47	162	19	127	3
ANU1875	Talasea	460	8068	14	53	175	21	139	3
ANU1879	Talasea	306	7651	14	54	130	19	130	3
ANU1880	Talasea	348	7712	14	57	131	19	136	3
ANU1882	Talasea	467	8355	16	53	185	21	138	4
ANU1883	Talasea	472	8202	15	55	179	21	136	3
ANU1943	Talasea	456	8538	15	53	179	21	138	3
ANU1951	Talasea	540	8593	14	55	183	21	140	4
ANU2365	Talasea	438	9526	15	56	125	29	154	4
ANU2366	Talasea	446	9552	14	56	124	29	154	4
ANU2367	Talasea	441	10020	16	57	128	28	158	5
ANU287	Talasea	433	8525	15	53	180	22	139	4
ANU380	Talasea	404	8945	16	58	112	27	138	4
Baki G001: 10	Baki	457	9811	17	53	121	28	150	5
Baki G001: 11	Baki	453	10498	15	59	130	30	160	5
Baki G002: 28	Baki	445	10328	15	56	131	29	158	5
Baki G017: 4	Baki	449	10014	16	54	126	29	153	5
Baki Garala 1	Baki	432	9663	15	53	121	27	148	5
Gulu 04: 08: 1	Gulu	311	8110	14	58	134	20	135	4
Gulu: 108	Gulu	313	9230	17	64	142	21	140	4
Hamilton G019: 2: 7	Hamilton	354	7036	16	56	134	17	131	4
Hamilton G023: 5	Hamilton	287	7297	16	58	130	18	135	4
ANU2362	Mopir	567	8631	14	37	169	27	127	4
ANU2372	Mopir	597	8978	16	38	174	28	131	4
Mopir East	Mopir	557	9128	16	35	164	27	127	5
Mopir Ulip Stream east 1	Mopir	593	9226	17	37	169	28	132	4
Mopir Ulip Stream east 2	Mopir	489	8083	14	34	151	24	117	5
ANU1131	Lou	563	18184	21	146	68	42	387	46
ANU1855	Lou	525	17911	20	144	69	41	383	45
ANU1856	Lou	574	17737	19	141	68	41	382	46
ANU1857	Lou	482	17582	19	141	67	40	374	45
ANU1859	Lou	478	16768	19	136	65	40	364	44
ANU2000	Lou	478	13554	18	138	61	38	296	40
ANU277	Lou	597	19922	18	121	81	43	404	46
ANU280	Lou	569	17068	18	138	66	39	369	44
ANU3885	Lou	451	16797	18	136	66	38	362	44
ANU4919	Lou	491	16516	19	137	62	39	360	43
ANU5272	Lou	514	16902	18	137	66	40	372	44
ANU2024	Pam	471	13364	18	149	41	40	264	43
ANU2027	Pam	477	13920	19	156	44	42	275	44
ANU2030	Pam	536	14919	19	152	48	39	273	42
ANU283	Pam	447	13741	20	154	42	40	267	42
ANU1899	West Fergusson	373	9700	19	125	69	25	282	10
ANU302	West Fergusson	359	9505	19	125	72	26	298	10
ANU303	West Fergusson	322	9243	18	130	60	27	274	10
ANU304	West Fergusson	383	9475	18	124	69	24	284	10
ANU305	West Fergusson	430	8111	19	128	102	22	194	9
ANU301	East Fergusson	683	21128	22	113	5	74	882	27
ANU306	East Fergusson	759	22213	22	118	4	77	918	27
ANU307	East Fergusson	802	26902	19	157	3	115	1465	43
ANU308	East Fergusson	738	21876	19	114	3	73	896	28
ANU309	East Fergusson	939	25172	22	129	4	63	605	25
ANU310	East Fergusson	944	27961	20	133	5	65	620	23

Text S1. Archaeological investigations at Waim

Waim village and its recent history

The Waim archaeological site is situated in the modern village of Waim, 1980m above sea level (asl) on the southern flank of the Bismarck Range and on the true right side of the Jimi River Valley (Figs. S8-S9). Geopolitically it is situated within the Jiwaka Province of Papua New Guinea, 60km NE of Mt Hagen and 140km WSW of the coastal town of Madang. The modern village of Waim village has 430 occupants living in around 80 households comprised of several extended family groups (as of the 2011 Census). It is noted by local residents, however, that the population in the Waim area during the late nineteenth and early-mid twentieth Centuries was small, and likely did not exceed 100-150 people.

Fig. S8. Grassland mountains and forested Jimi River Valley landscape below Waim, looking south, with the Jimi-Wahgi divide in the background. April 2016. Photo Credit: Ben Shaw, UNSW.

European contact with the people of the Waim area was not made until the mid-20th Century, despite parts of the Jimi Valley having been explored from 1933 onwards (*21, 54, 55*). In 1953-54 contact had been made with communities in both the Kaironk and Simbai Valleys (*56, 57*), and by 1958 patrol officers in the Jimi Valley had made contact with most of the remote communities along the Bismarck Range, including Waim (*58, 59*). Prior to this time, knowledge of outside influences on the north coast throughout the 19th Century would likely have reached Waim area, but direct influence through the trade of European goods would have been fleeting or non-existent. (*14, 20, 57, 60-62*).

Site discovery

Waim was first recorded as an archaeological site when the village was visited by Ben Shaw on the 10-11th April 2016, during the second field season in the Simbai-Kaironk area as part

of the Australian Research Council funded 'Pathways into the interior' archaeological project. Community leaders from Waim had informed the archaeological team that several stone artefacts had been found in the village area over the past several years and had requested an archaeological assessment of the area to ascertain the antiquity of the objects.

Fig. S9. The Waim site, looking east, situated on a natural hill top within Waim village. North and south direction is annotated. Note the person standing in from of the hill for scale. April 2016. Photo Credit: Ben Shaw, UNSW.

Archaeological investigations at the Waim site

April 2016: Survey and test pits

Foot survey of the Waim village area indicated that archaeological potential was higher towards the northern edge of the hilltop where the sedimentary profile remained intact (Fig. S9). By contrast, eroding base rock was exposed in several places along the southern extent of the hilltop where only a remnant sedimentary deposit was identified. Similarly, base rock was extensively exposed further to the north at the lower end of the slope where the basal clay deposit had recently been turned over for gardening. A 55x60cm test pit was dug into a partially exposed section along the northern face of the hilltop top. Flaked lithic material was recorded throughout the 65cm deep deposit, with a notable concentration of lithic flakes 48-50cm below the surface. A pestle fragment was also uncovered at this depth (Fig. S10).

August 2016: Test pitting and systematic excavation

The sub-surface nature of the archaeological deposit was initially defined by a single test pit. Upon return to Waim in August 2016, five 50x50cm test pits were dug across the top of the hilltop to identify the extent of the archaeological deposit in this area and to compare it to the

stratified section identified in April. The test pits confirmed that the top of the hilltop offered limited archaeological potential, with deeper cultural deposits concentrated along the N and NW side (Fig. S11).

Square A, C and F

Squares A, C and F were excavated separately but immediately adjacent to each other into the partially exposed section on the northern side of the hilltop. Prior to excavation loosely compacted clay overburden was removed and discarded, exposing the buried topsoil. Square A was placed 40-140cm to the east of the April test pit to incorporate a large lithic artefact partially exposed in the section (Shown in Fig. S11). Square C was subsequently excavated and included the intact deposit around the test pit dug in April to further define the stratigraphic context of the pestle base fragment. Square F was excavated to the north of Square C to define the nature of the archaeological deposit at the base of the slope, and investigate a ditch feature which had been partially exposed in Squares A and C (Fig. S12).

Squares B and D

Square B was placed on the northwestern side of the hilltop when the partially exposed section was cleaned back and a large lithic artefact was identified *in situ*. Square D was a subsequent 0.5x1m extension of Square B to better understand the geomorphology relating to sedimentary accumulation at the base of the hilltop (Fig. S13).

Fig. S10. Excavation of the test pit showing the gabbro pestle fragment and other lithic artefacts exposed in the front (northern) half of the square. Scale: 50cm. April 2016. Photo Credit: Ben Shaw, UNSW.

Fig. S11. Partially exposed section that had been previously cut back by Waim residents around the northern edge of the hilltop. It was cleaned back prior to excavation. The re-excavated April test pit can be seen in the background, which was later incorporated into Square C. A large stone can be seen protruding from the section - a cached axe-adze preform later exposed in Square A. Note the modern stone features. Much of the stone for these was sourced from the area during ground clearance, much of it had been culturally modified. August 2016. Photo Credit: Ben Shaw, UNSW.

Fig. S12. Square F after excavation showing a possible posthole feature in the lower right hand corner. The remainder of the square base consisted of natural stone. Photo Credit: Ben Shaw, UNSW.

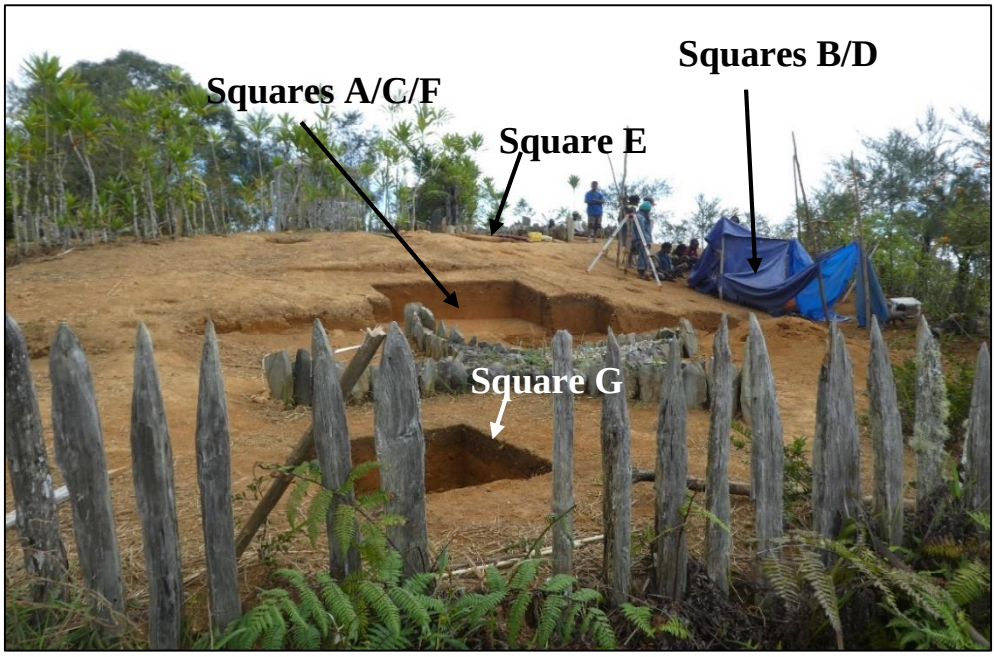

Fig. S13. The Waim site with the locations of the systematically excavated squares shown. Photo Credit: Ben Shaw, UNSW.

Square E and G

The accumulation of cultural material was found to be considerably higher at the base of the spur apex, and it was becoming apparent that the angle of the modern slope was different to that of the basal clay slope because of long term sediment accumulation during prehistoric occupation. Square E was therefore placed just on top of the slope midway between the Squares A-C-F and Squares B-D excavation areas so that the stratigraphic profiles could be correlated. Square G was excavated on the flatter land immediately to the north of the hilltop to determine the nature and extent of the cultural deposits away from the base of the slope (Fig. S13).

Text S2. Stratigraphic descriptions of sedimentary layers at Waim

Stratigraphic layers were identified during and after excavation by differences in texture, colour, consolidation and particle size.

Layer 4 (Munsell: 7.5YR 6/7) is a culturally sterile fine silty clay matrix, with enclosing charcoal dated to 9900-9650 cal. BP (Beta-450802; 95.4% range).

Layer 3 (7.5YR 4/6) is dated to 7450-7250 cal. BP (Beta-450806), comprised a clayey silt identified only in Square B/D. Layer 3 provides the earliest unequivocal evidence for a human presence at Waim. A ditch feature, possibly a drainage channel, was cut into Layer 4 a millennium later (6450-6300 cal. BP, OZU323) but yielded no material culture.

Layer 2c (7.5YR 5/7) is a coarse sandy silt accumulated on the side and at the base of the pronounced apex slope.

Layer 2b (7.5YR 5/6) is a sandy silt with an increased concentration of lithic artefacts relative to Layer 2c.

Layer 2a (7.5YR 5/6) is a sandy silt, less compact compared to 2b-c.

Layer 1 (7.5YR 5/8) comprises a thin deposit of coarse silty clay re-deposited during modern topsoil clearance of the spur apex, and derived from Layer 2a-c.

Text S3. Technological and geological characteristics of the Waim lithics

The stone raw materials documented at Waim largely reflect the local geology of the Kompiai Formation which Bain and Mackenzie (*45*) describe as "dark grey siltstone, light grey laminated greywacke siltstone and sandstone, dark grey phyllitic shale, schistose shale, maroon phyllite, and dark grey highly indurated cleaved shale". The assemblage is dominated by siliceous argillite and siltstones which comprise approximately 81% of the total assemblage. These stone raw materials are broadly similar to each other, only differing in level of silicification and grain size. It is possible that they originate from the same source. The colours range from cream to light grey to dark grey to brown. The silicification of these sedimentary rocks is likely to be a thermally metamorphic process associated with contact with intrusives (similar to that described for the Highland axe-adze quarry materials located just to the south of Waim (*20*)). Other local materials include maroon shale and greywacke.

The siliceous argillite/siltstone has also been ethnographically recorded in Highland axe-adze quarries located to the south of Waim. A reference collection from these quarries would be required for comparison. While the origin of this stone type cannot be clearly determined, it is parsimonious to attribute a local origin to the stone raw materials.

Volcanic and plutonic stone is present in the assemblage, including diorite, gabbro, microdiorite, crystal tuff and vitric tuff. The plutonic materials of diorite, gabbro and microdiorite are likely to be from the nearby Oipo Intrusives which are described as "gabbro, granodiorite, tonalite, dolerite, diorite, pyroxenite, and lamprophyre" (*45*) or the Marum Basic Belt, although this lacks diorite. The volcanic tuff material may derive from the Kana Volcanics or Hagen Volcanics, both of which are recorded as having tuffs.

Overall the assemblage contains a range of lithic material, including tools, flakes and angular fragments, although few cores are present. Evidence for axe-adze manufacture from the siliceous argillite/siltstone material includes a large block with cut marks indicating the use of sawing to cut the block into a desired preform shape (Square B Layer 2b). Sawing has been recorded ethnographically at some (but not all) quarries (*63*). Ground stone fragments are also present, as well as two flakes that show grinding on their dorsal surfaces, and a third flake that shows evidence for crushing or hammerdressing on its dorsal surface. Numerous greywacke pieces with abraded surfaces (as well as a large number of small fragments without abrasion) would also appear to have been used in the grinding process.

One complete axe was recovered in Square G Layer 2c, and was made from siliceous argillite/siltstone. This axe is very small and has a lenticular cross section. A lenticular axe fragment, made from siliceous argillite, was also recorded as a surface find. These two axes differ from the planilateral axe-adzes indicated by the cut stone preform. The large axe-adze preform and slab of raw stone recovered in Square A were analysed at the National Museum and Art Gallery of Papua New Guinea where they have been curated. Apart from axe manufacture other tool types present. Retouched flakes and fragments, as well as used flakes/fragments occur largely produced from siliceous argillite/siltstone. A core, subsequently used as a hammerstone, is made from the same raw material. Other tool types include a carved stone manufactured from gabbro (Square B Layer 2b), an incised stone of weathered volcanic rock that appears to have ochre residues on the surface (Square B Layer 2c), two pestles made from diorite and diorite-gabbro, a pyroxenite "matchstone", and a large diorite stone with a groove on one surface, perhaps used in tool manufacture

Text S4. Microwear analysis of carved and modified lithic artefacts

Fragment of carved face (Square B, Layer 2b).

This broken stone carving appears to be a fragment of what was once a carved face, where the right eye and brow ridge above the right eye are mostly intact (Fig. S14A-E). The carving was prepared by hammer dressing (pounding), which has resulted in several different stone textures across the surface (on the face margin, head, eyebrow and ridges) resulting from pitting and surface levelling (Fig. S14F-H).

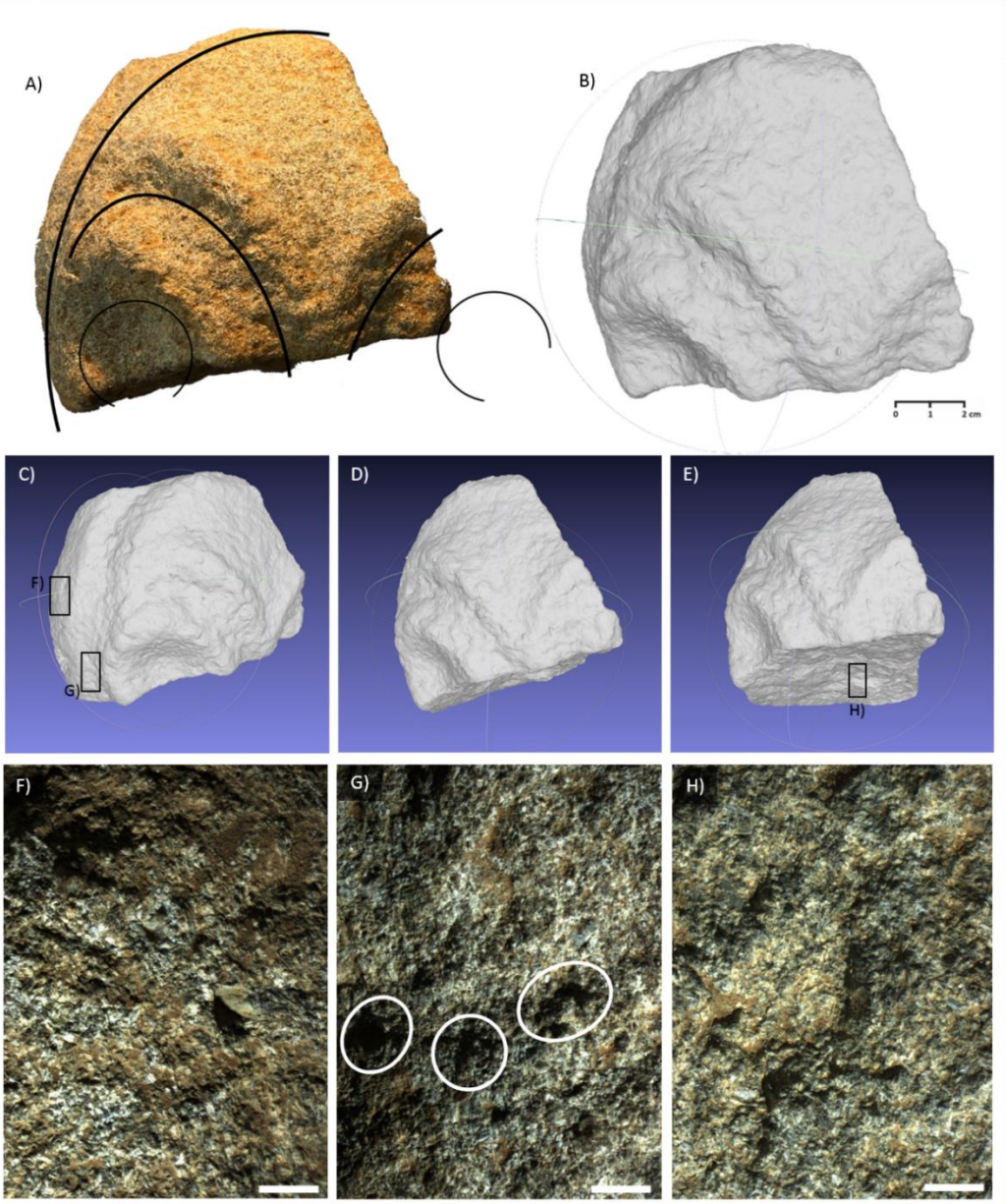

Fig. S14. Stone carving from square B, layer 2b. (A) Photograph of the stone with interpretation of carved relief features on prepared surface; (B) 3D scanned image surface of the stone at the same magnification and angle as (A); (C-E) 3D scanned images of the stone at various angles; (F) Detail of the surface texture of the smoothed zones, note that the surface is comparatively more levelled; (G) Detail of the surface texture from within the grooved zones, note the pitting (white circles) to deliberately roughen the surface; (H) Detail of unmodified broken stone surface. Scale bars for micrographs is 2mm. Photo and Figure credits: Richard Fullagar and Ebbe Hayes, University of Wollongong.

Incised stone (Square B, Layer 2c).

This relatively soft stone has two worked surfaces with deep, macroscopically visible grooves that have been deliberately carved into the surfaces, initiated from the edges. Surface 1 has three distinctive grooves (Fig. S15A) One of these appears to be natural feature/crack in the stone, and is oriented in a different direction to the other two grooves, which are deeply incised to maximum depth of ~5mm (Fig. S15A-C). The edges of the grooves are straight and have a "U" shaped cross-section near the edge and for most of their length, becoming more "V" shaped as they extend further across the stone surface and at their termination (Fig. S15D-F). Surface 2 also has two roughly parallel grooves, but these appear to be less deeply incised compared to those on Surface 1 and consistently have a "V" shaped cross-section (Fig. S15G-H). The straight edges of the grooves and their depth indicate that that they were probably formed by sawing with a harder stone to form the grooves. The "U" cross-section suggests another softer material (e.g. plant fibres) may have been worked inside the grooves after they were initially created with stone. Organic residues were also documented in, or close to the grooves. Plant fibres were also documented beneath the layers of sediment, indicating that they were present on the stone prior to deposition (Fig. S15I-J).

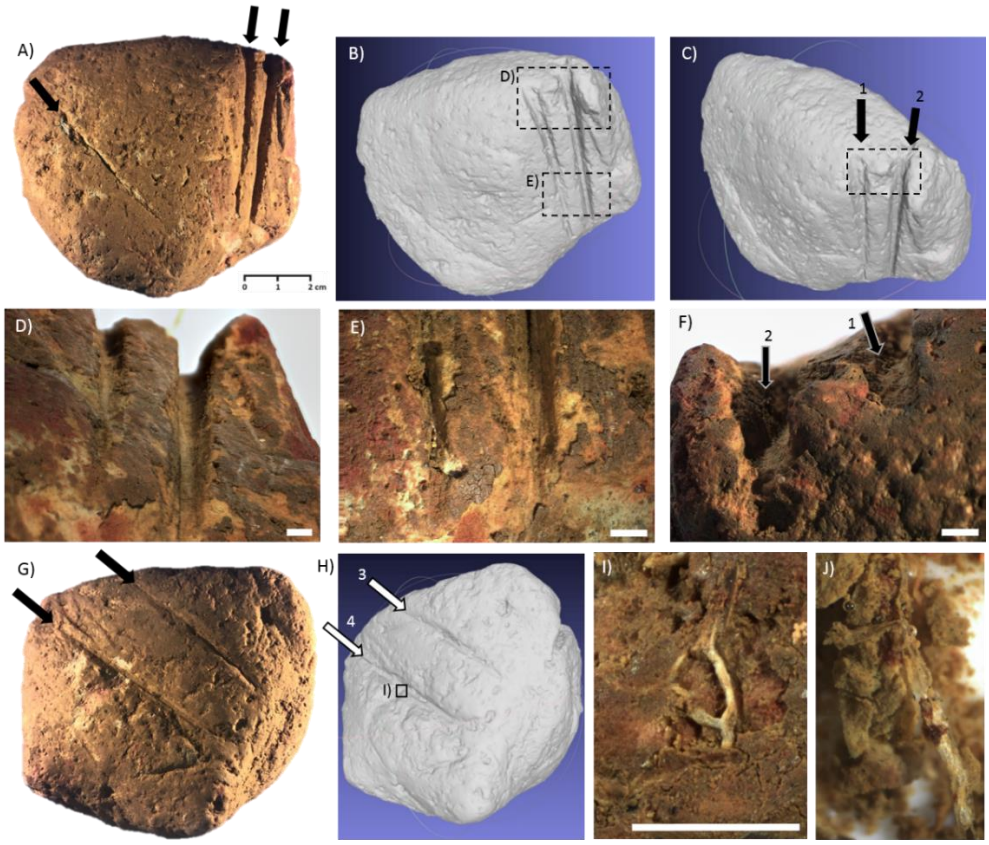

Fig. S15. Artefact with incised cut/groove marks, from square B, layer 2c. (A-C) Photograph and 3D scanned image of Surface 1; note the three distinctive grooves, two of which have been deliberately incised; (D) "U" shaped cross-section of grooves on Surface 1, near the edge of the artefact; (E) "V" shaped cross-section of the grooves on Surface 1 near their termination; (F) alternate view of "U" shaped grooves on Surface 1 (photographed horizontally from inset in (C)); (G-H) Photograph and 3D scanned image of Surface 2; note the two distinctive grooves with a "V" shaped cross section; (I) plant fibre documented near Groove 4, underneath the sediment; (J) plant fibres were identified in water used to remove sediment. Artefact scale bar is 2cm; micrograph scale bars are 2mm. Photo and Figure credits: Richard Fullagar and Ebbe Hayes, University of Wollongong.

Ground pestle base (Square F, Layer 2b).

A near-complete ground pestle base (convex in section) has a pitted surface resulting from pounding as well as levelled zones with fine striations (Fig. S16A-C). The striations are generally oriented in the same direction and are the result of stone-on-stone contact. Documented residues include decayed rootlets and other fibres, but these mostly occur above the sediment and therefore are likely to be post-depositional and not related to use.

Ground pestle base fragment (Square C, Layer 2c).

A ground pestle fragment has a part of its base (convex in section) and lower shaft remaining (Fig. S16D). The base has both pounding and grinding wear, indicated by the presence of pits and fine striations within the levelled zones (Fig. S16F). The texture of the shaft is not as smooth as the base—the result of having fewer levelled zones. Striations are also absent along the shaft but pitting is common, indicating stone-on-stone contact from manufacture or use (Fig. S16E).

Pyroxenite fragment with striations (Square D, Layer 2b).

This pyroxenite fragment has grinding wear on one surface (convex in section) that is characterised by deep scratches, oriented in mostly the same direction and are visible macroscopically (Fig. S16G-H). Under very high magnification (x200), fine striations are also visible and are orientated in multiple directions (Fig. S16I). Both the scratches and finer striations indicate stone-on-stone grinding.

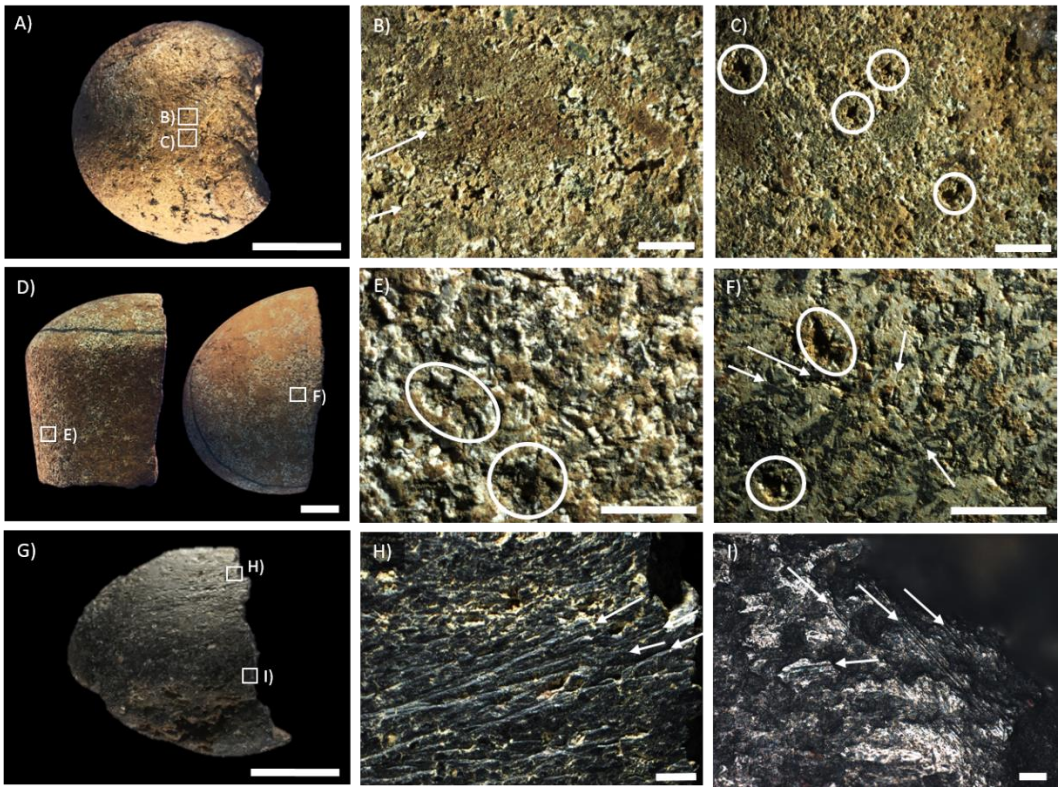

Fig. S16. Ground-stone fragments and corresponding microwear from various squares of the Waim excavations. (A-C) Near-complete ground pestle base from Square F, Layer 2b; (D-F) Ground pestle base fragment from Square G, Layer 2c; (G-I) ground pyroxenite fragment from Square D, Layer 2b. Artefact scale bars are 2cm; micrograph scale bars are 2mm; micrograph scale for (O) is 0.05mm. White arrows indicate direction of striations; white circles indicate pitting. Photo and Figure credits: Richard Fullagar and Ebbe Hayes, University of Wollongong.

Text S5. Geometric morphometric analysis of ancient starch from Waim

Background

A visual comparison/maximum dimension approach has been the basis of most starch grain identifications previously presented in the literature (e.g. *64, 65*). It is a subjective approach to the study of starch, and there have been few methodological advances in this area to move the discipline forward, primarily because of the challenges inherent to the study of starch. Starch grains are probably the most difficult plant microfossil to identify because the majority of starch grains are very difficult to discriminate from one another. A new approach was needed, and to this end the geometric morphometric method for starch identification was developed (*13*).

The geometric morphometric method is a robust statistical technique formulated, in this application, to provide a high level of confidence in attributing unknown starch grains to plant taxa (*13, 41, 66*). The method has been applied to archaeological problems in different contexts to further our understanding of plant exploitation associated with ground stone implements in prehistory (*41, 67, 68*).

The study of plant microfossils is grounded in comprehensive modern comparative reference collections of known economic and non-economic starchy plants for the area under study (*69*). The reference set compiled for the Waim study included *Dioscorea pentaphylla, D. bulbifera, D. alata, Castanopsis acuminatissima*, Zingiberaceae, *Musa ingens*, *Hydriestele*, sp., *Colocasia esculenta*, *Saccharum officinarum*, *Pueraria lobata* and *Psophocarpus tetragonolobus* (Fig. S17). Other possible species including *Elaeocarpus womersleyi* were not available at the time of this study.

Micrographs of individual starch grains were digitised using a graphical user interface (GUI) developed in MATLAB (MATLAB Release 2014b, The MathWorks, Inc., Natick, MA, USA), and a WACOM Intuos Pen Tablet (CTH-480). The outline of the starch grain is referred to as the region of interest (ROI) and the location of the hilum position (growth centre) was also marked. Other grain surface features such as fissures and lamellae were also recorded.

Classifier details for reference starch

Following the methods of Coster and Field (*13, 66*), the optimal classifier developed for this study of ancient starch was a quadratic discriminant with a voted output based on 3 subgroups of each species. The predictor variables were the area, circle metric, and the first six Fourier components of each grain. A dendrogram (Fig. S18) shows the separation of the reference set using these predictor variables. The easiest starch reference taxa to separate was *Dioscorea pentaphylla* and the most difficult to separate from each other were *Pueraria lobata* and *Psophocarpus tretragonolobus.* The confusion matrix for this reference set (Fig. S19) shows the target class (the known species in the reference set) and the output class (those predicted by the classifier). The numbers of grains classified for each target-output pair in the reference set are reported (and as a percentage the total grains below in each entry). The accuracy (correct and incorrect) levels of each row and column are shown at the right and bottom.

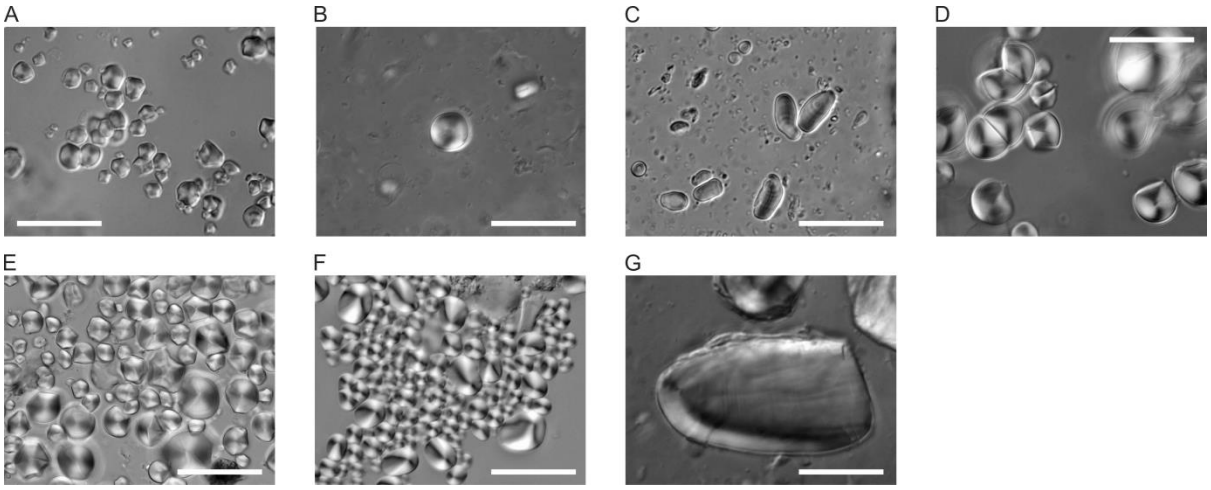

Fig. S17. Comparative reference starch used in this study and not shown in fig. S20. More than 100 grains from each sample was digitised for the analysis. These images are representative only and do not show the range of variation that is present across the sample. A. *Dioscorea bulbifera*; B. Zingiberaceae; C. *Musa ingens*; D. *Hydriestele*, sp.; E. *Colocasia esculenta*; F. *Pueraria lobata; G. Psophocarpus tetragonolobus*. Photo and Figure Credits: Judith Field, UNSW.

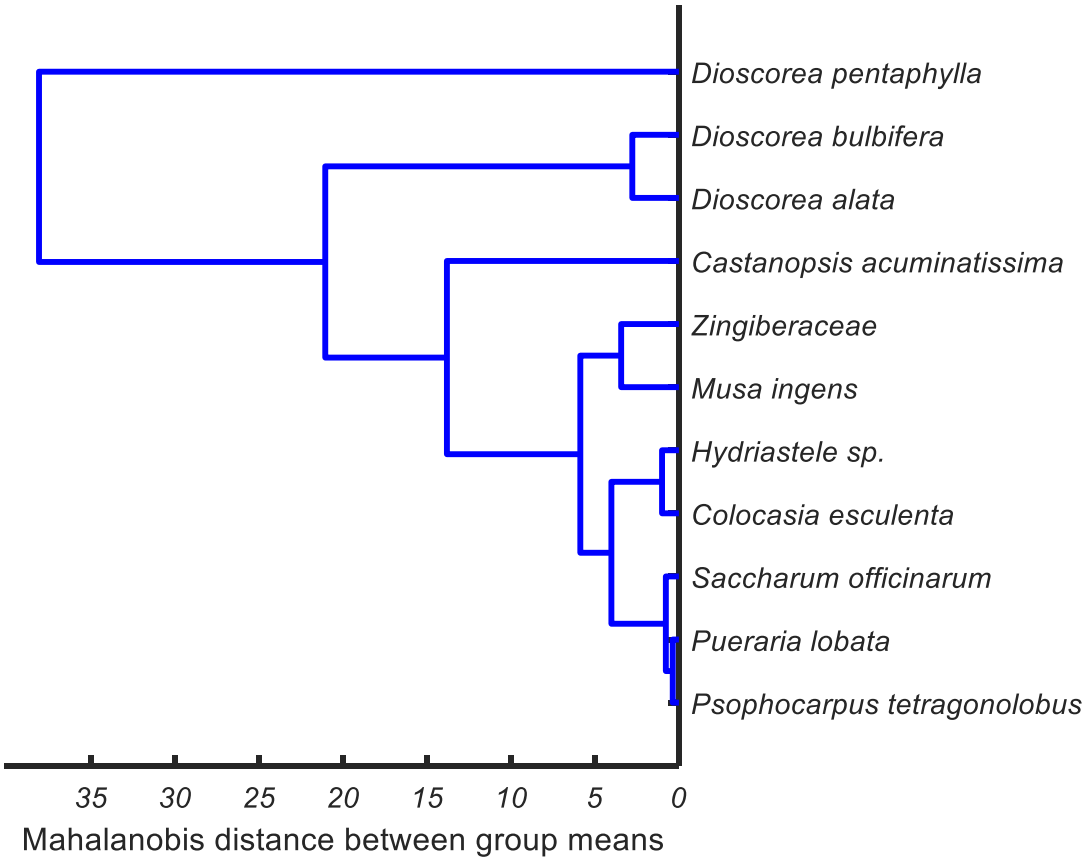

Fig. S18. Dendrogram for the optimal classifier—a quadratic discriminant—showing the Mahalanobis distance between the means of the species. The optimal classifier included the area, circle metric, and the first six Fourier components of each grain. Note that *Pueraria lobata* and *Psophocarpus tetragonolobus* were the most difficult to separate (*41*). Figure Credit: Adelle Coster.

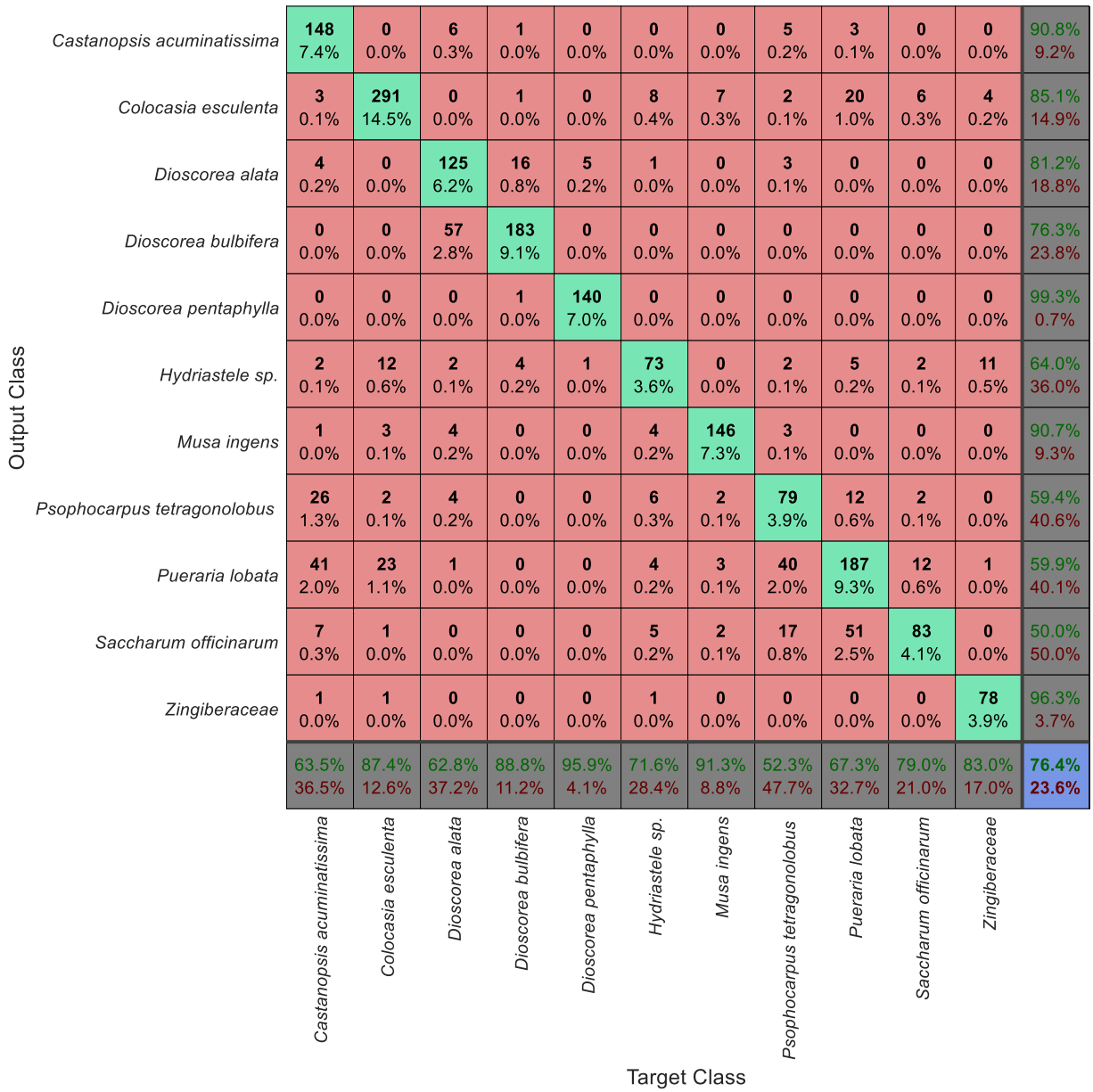

Fig. S19. The confusion matrix for the reference species used in the study. The optimal classifier was a quadratic discriminant with a voted output based on 3 subgroups of each species. The target class is the actual (known) reference species, and the output class is the species predicted by the classifier. The numbers of grains classified for each 'target-output pair' of the reference set are reported in each square (and as a percentage the total grains below in each entry). The accuracy (correct and incorrect) for each output class is shown at the end of each row and for each target class column at the bottom. Note that the reference set contained different numbers of grains for the different species. The confusion matrix is one indicator of the confidence for the predictions for each species (other measures include the reverse cross- fold validation error and Positive Prediction Value (*PPV)* and are described in detail elsewhere (*41, 66*)). Figure Credit: Adelle Coster.

Plant taxa identified on pestles and soil at Waim

The frequencies of starch grains recovered varied significantly between the two pestles, and the soil sample (Table S4). *C. acuminatissima* was the most common taxa identified on the pestles and in the soil sample, though the concentrations/cm^3 in the soil sample were significantly lower. Pestle 1 (Square C) yielded the highest number of starch grains (85), the most abundant being *C. acuminatissima*, followed by *Hydriastele* sp. and *Musa ingens*, with

small contributions from *S. officinarum*. The Pestle 2 (Square F) starch assemblage was comprised mostly of *C. acuminatissima* and *D. alata*, with contributions from *D. pentaphylla* and *P. lobata.* Of the 12 grains identified in the soil sample, the most prevalent identification was to a specific plant taxa: *C. acuminatissima*. We have used a very conservative approach for the identification of starch grains to plant taxa, and in this case the numbers were relatively low. The remaining unidentified grains can be explained by either: 1. They belong to species in the reference set but failed to meet our stringent conditions for inclusion, or 2: belong to other species not in our reference set that are yet to be identified. Examples of the some of the species included in the reference set are shown in Fig. S20.

The reference set was re-substituted into the classifier to determine the classifier score corresponding to different proportions of the true positive classifications for each species, termed the Positive Prediction Value (*PPV) (41, 66)*. The scores for unknown grains with a *PPV* corresponding to greater than 90% true positive classifications were deemed confident predictions (so not any other species in the reference set), and those corresponding to a *PPV* between 80% and 90% were deemed probable. Overlaid with this assessment of confidence is the rCVE, or reverse cross-fold validation error for the classifier and reference set, where increasing rCVE indicates decreasing confidence. All predictions were also visually verified by a starch expert (J.F.).

Table S4. Numbers of grains identified of each of the comparative reference species. The rCVE (reverse cross-fold validation error) for the identification is also shown – the greater the rCVE, the less confident the identification/separation from its closest species. Those above the threshold level of 0.3 are deemed not confident and are indicated by the shaded background (see also Figs. S18-S19). The number of grains with confident and probable (bracketed) predictions (according to their *PPV*) are listed. Table Credit: Judith Field, UNSW.

	Total Grains Found	*Dioscorea pentaphylla*	*Zingiberaceae*	*Musa ingens*	*Colocasia esculenta*	*Castanopsis acuminatissima*	*Dioscorea bulbifera*	*Dioscorea alata*	*Hydriastele sp.*	*Pueraria lobata*	*Psophocarpus tetraqonolobus*	*Saccharum officinarum*
CVE		0.04	0.04	0.15	0.18	0.23	0.29	0.29	0.43	0.49	0.56	0.63
SIM 18 Pestle 1	85	-	-	-(7)	-	9(-)	-	-	8(5)	-	-	-(1)
SIM 18 Pestle 2	26	2(-)	-	-	-	6(-)	-	6(-)	-	1(-)	-	-
Soil	12	-	-	-	-	3(-)	-	-	-	-	-	-

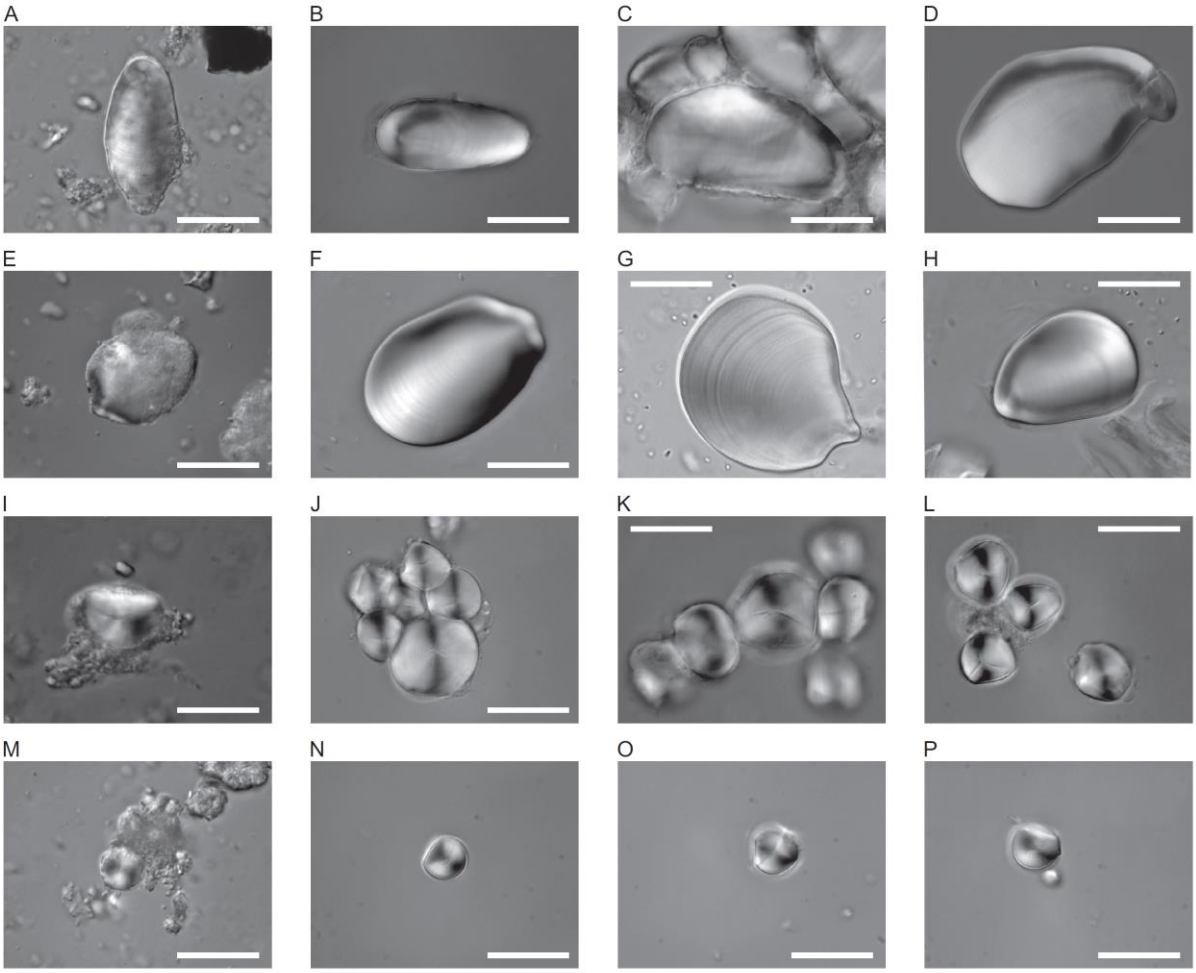

Fig. S20. Archaeological starch (**A**, **E**, **I**, **M**.) and their correlating species identification (in the 3 images to the right). The identification of the unknown starch grains used a quadratic discriminant classifier. Only confident identifications were included. Image A was identified as *Dioscorea alata*, shown here with the comparative reference set (**B**-**D**). Image E was identified as *Dioscorea pentaphylla*, **F**-**H** are *Dioscorea pentaphylla* images from the reference set; Image I was identified as *Castanopsis acuminatissima*, N-P are *Castanopsis acuminatissima* images from the reference set Image M was identified as *Saccharum officinarum*, N-P are *Saccharum officinarum* images from the reference set. Scale bar is 20 µm. Photo and Figure Credits: Judith Field, UNSW.

Text S6. Phytolith analysis of pestle and sediments from Waim

One pestle sample (SIM 18, Pestle 1) was studied for phytolith remains extracted from the used surface of the pestle. To further assess whether or not the artefact phytolith assemblage was contaminated with phytoliths from adjacent sediments, a sample from the adjacent sediment matrix was also analysed. The starch and phytolith assemblages were extracted from the same samples.

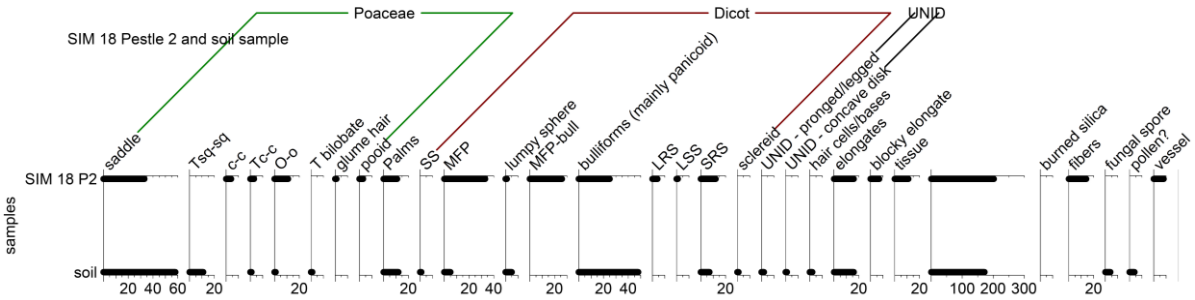

Fig. S21. Phytoliths identified on the Waim pestle and sediment. Figure Credit: Lisa Kealhofer.

The results indicate that the Pestle artefact sample includes phytoliths from both sediments and use (Fig. S21). In general, the pestle grass assemblage strongly overlaps with the sediment grass assemblage (Bambusoid saddles, other short cells [Tsq-sq] as well as bulliforms), although the presence of a few distinctive forms suggests possible direct contact with grasses [ovoid forms]. The palm assemblage is also very similar between the two samples. In each of these cases (as for the elongates), the frequency is greater in the soils than on the pestle. SRS (small round sphere) phytoliths were slightly more abundant on the pestle than in the soil sample; they are produced in a variety of taxa, including Euphorbiaceae and Dioscoreaceae. However, the distinctive multifaceted polyhedral forms [MFP & MFP bulliform-shape] found on the pestle are either rare or absent in the sediment samples. These appear, therefore to most convincingly represent economically processed taxa. Similarly, the larger tissue fragments identified in the pestle sample indicate plants not found and/or preserved in the soil sample.

The MFP forms do not directly match our current reference material. More generally, such forms are produced by *Flacourtia* sp., *Castanopsis* sp., and *Annonaceae* species, most of which have edible fruits. The presence of *Castanopsis* sp. type starch suggests this might be a likely source. If the SRS are not soil contaminants, they may support the *Dioscorea*/yam starch identification. The larger fragments of tissue provide additional evidence that soft plants were processed/in contact with the pestle.

The soil sample, alone, reflects an open grassy environment and with limited evidence [palms and a low percentage of MFPs] for an arboreal or even shrubby component.

Text S7. pXRF reference data and principal components analysis of Waim obsidian

Table S5 demonstrates the precision of the University of Otago pXRF spectrometer. Table S6 shows the elemental loadings on Components 1, 2, and 3. Niobium loads heavily on both the first and second component, allowing separation of sources on both the X and Y-axis; Zirconium also loads heavily on the 1st Component. Rubidium (Rb) loads heavily on component 3, allowing for clear separation between Talasea and Mopir sources along the Y-axis. The three components make up 98% variation, confirming very good definition of the source groupings. The Waim obsidian sample clusters with the Kutau/Bao source from the Talasea region, New Britain.

Table S5. Error range of Bruker Tracer III-SD during analysis, using the U.S. Geological Survey BHVO-2 Geological Standard. Table Credit: Anne Ford.

	Mn	Fe	Ga	Rb	Sr	Y	Zr	Nb
USGS (ppm)	1290	86300	21.7	9.8	389	26	172	18
UoOtago Average (ppm) (n=14)	1094	79741	26.92	14.94	337	23.19	152	16.3
Std Dev	40.67	866.91	1.29	0.59	6.65	0.84	3.20	0.61
RSD (%)	3.72	1.09	4.79	3.92	1.98	3.61	2.11	3.72

Table S6. Elemental loadings of three components (98% variation) for analyzed obsidian source samples and the Waim obsidian flake. Table Credit: Glenn Summerhayes.

	1	2	3
Mn	0.7	0.21	0.09
Fe	-0.12	0.1	0.05
Ga	0.12	0.11	-0.05
Rb	-0.17	-0.11	-0.18
Sr	1.3	-0.19	0.01
Y	-0.16	0.17	0.06
Zr	-0.37	0.13	-0.07
Nb	-0.68	-0.42	0.09